# A New Consistent Spatial Differencing Scheme for the Transonic Full-Potential Equation

Jolen Flores,* Terry L. Holst,* Dochan Kwak,† and Duane M. Batiste‡
*NASA Ames Research Center, Moffett Field, California*

**A new spatial differencing scheme for the transonic full-potential equation in conservative form has been developed. Three consistency conditions for the full-potential equations are derived and are satisifed by the new scheme. This scheme guarantees zero truncation error on any curvilinear mesh for freestream flows in either two- or three-space dimensions. Solutions obtained with this new differencing scheme, away from freestream regions, exhibit greatly improved accuracy, especially for nonsmooth or singular meshes. The computing times associated with the new scheme are approximately the same as the less accurate old scheme when computations are performed on the same mesh.**

## Introduction

GRID-generated irregularities such as singularities, rapid stretching, and coarseness manifest themselves in many realistic configurations. Examples of rapid stretching and skewness can be seen at airfoil trailing edges when the "O mesh" mapping topology is used. In multicomponent configurations (e.g., multielement airfoils, wing/fuselage configurations, or wing/fuselage/pylon/nacelle configurations) grid singularities, rapid stretching, and cell skewness abound. Ideally, we desire a stable flow-solver algorithm that can handle all of the aforementioned irregularities, yet provide uniform accuracy over the entire mesh.

In the present formulation, large improvements in accuracy are obtained in two ways: 1) global improvements which arise from the perfect capture of the freestream, and 2) local improvements near grid singularities. The last improvement is helpful when problems with inherently nonsmooth meshes are considered.

The new scheme uses a numerical evaluation of the mapping metrics—a procedure which in itself is not new. The new aspect of the present approach is the way in which the metrics are evaluated. It can be shown analytically or numerically that if the metric differencing is arranged appropriately, the truncation error associated with a freestream distribution of the dependent variable is zero. This type of procedure was discussed by Pulliam and Steger[1] for the Euler equations but essentially was not used because of the small improvements in accuracy obtained on smooth meshes. Thomas and Lombard[2] developed a geometric conservation law (GCL) which linked the finite difference and finite volume methods of flow computations. They presented numerical results, for both implicit and explicit difference schemes, to verify the GCL concept. Hindman[3] also showed that geometrically induced errors could occur when the consistency condition was violated.

Received Dec. 10, 1982; presented as Paper 83-0371 at the AIAA 21st Aerospace Sciences Meeting, Reno, Nev., Jan. 10-13, 1983; revision received Aug. 25, 1983. This paper is declared a work of the U.S. Government and therefore is in the public domain.

*Research Scientist, Applied Computational Aerodynamics Branch. Member AIAA.

†Research Scientist, Applied Computational Aerodynamics Branch.

‡Co-op Student, Applied Computational Aerodynamics Branch.

All of the work previously mentioned was performed on the Euler equation formulation. Chattot et al.[4] developed a spatial difference scheme which contained a perfect freestream capture characteristic for the full-potential equation. However, this formulation used a form of the full-potential equation that was not written in strong conservation law form (i.e., the metrics were written outside the main flux differentiation). On smooth meshes this formulation behaves like the conservation law form, but on nonsmooth meshes such a scheme may suffer in accuracy because the metric variation is not included in the flux differentiation. Jameson and Caughey[5] developed a spatial difference scheme for the full-potential equation written in strong conservation law form. This finite volume scheme, as it is called, possessed the perfect freestream capture capability but had the disadvantage of allowing oscillatory solutions (i.e., odd-even grid point decoupling). This problem was corrected by adding a "compensation flux" to each flux calculation, which effectively shifted the flux evaluation position and corrected the odd-even solution decoupling, but unfortunately removed the perfect freestream capture capability.

In this study several spatial differencing schemes for the conservative full-potential equation are discussed. Simple consistency conditions that guarantee the perfect capture of freestream flow are presented. Results computed using several different spatial differencing schemes (some that satisfy the consistency conditions and some that do not) on a simple two-dimensional model problem are presented and discussed. To analyze the sensitivity of the various spatial differencing schemes, studies have been conducted for transonic flow over a two-dimensional cylinder. Different grid irregularities are imposed, and comparative results are shown which illustrate their effects on the solution. Finally, transonic airfoil results with the new and old schemes are presented and discussed.

## Theoretical Background

### Full-Potential Equations

The full-potential equation written in strong conservation law form is given by

$$(\rho\phi_x)_x + (\rho\phi_y)_y = 0 \tag{1a}$$

$$\rho = \left[1 - \frac{\gamma-1}{\gamma+1}(\phi_x^2 + \phi_y^2)\right]^{1/\gamma-1} \tag{1b}$$

where the velocity components ($\phi_x$ and $\phi_y$) and the density $\rho$ are nondimensionalized by the critical sound speed $a_*$ and the stagnation density $\rho_s$, respectively; $x$ and $y$ are Cartesian coordinates, and $\gamma$ is the ratio of specific heats.

Mass conservation is expressed by Eq. (1) for flows which are isentropic and irrotational. For many transonic flow applications, the corresponding shock-jump conditions are valid approximations to the Rankine-Hugoniot relations.[6]

To transform Eq. (1) from the physical domain (Cartesian coordinates) to a computational domain, a general, nonorthogonal, independent variable transformation is used. This general transformation

$$\xi=\xi(x,y) \qquad \eta=\eta(x,y) \tag{2}$$

maintains the strong conservation law form of Eq. (1). The full-potential equation written in the computational domain ($\xi-\eta$ coordinate system) is given by

$$(\rho U/J)_\xi+(\rho V/J)_\eta=0 \tag{3a}$$

$$\rho=\left[1-\frac{\gamma-1}{\gamma+1}\left(A_1\phi_\xi^2+2A_2\phi_\xi\phi_\eta+A_3\phi_\eta^2\right)\right]^{1/\gamma-1} \tag{3b}$$

where

$$U=A_1\phi_\xi+A_2\phi_\eta \qquad V=A_2\phi_\xi+A_3\phi_\eta \tag{4}$$

$$A_1=\xi_x^2+\xi_y^2=\nabla\xi\cdot\nabla\xi$$

$$A_2=\xi_x\eta_x+\xi_y\eta_y=\nabla\xi\cdot\nabla\eta$$

$$A_3=\eta_x^2+\eta_y^2=\nabla\eta\cdot\nabla\eta \tag{5}$$

and

$$J=\xi_x\eta_y-\xi_y\eta_x=1/(x_\xi y_\eta-x_\eta y_\xi) \tag{6}$$

The variables $U$ and $V$ are the contravariant velocity components along the $\xi$ and $\eta$ directions, respectively; $A_1$, $A_2$, and $A_3$ are metric quantities, and $J$ is the Jacobian of the transformation. The following metric identities are necessary in numerically evaluating the preceding expressions.

$$\xi_x=Jy_\eta \quad ,\xi_y=-Jx_\eta, \quad \eta_x=-Jy_\xi, \quad \eta_y=Jx_\xi \tag{7}$$

**Operator Notation**

The difference-operator notation used in this report is briefly described in this section. Only the $\xi$-direction operators will be presented, as the operators in other directions can be obtained by symmetry. Standard second-order-accurate central-difference operators are defined by

$$\delta_\xi(\ )_{i,j}\equiv\tfrac{1}{2}[(\ )_{i+1,j}-(\ )_{i-1,j}] \tag{8}$$

where the $i,j$ subscripts indicate position in the finite difference mesh. For convenience, the $\Delta\xi$ increment is unity and, therefore, is omitted.

One-sided difference operators are defined by

$$\vec{\delta}_\xi(\ )_{i,j}\equiv(\ )_{i+1,j}-(\ )_{i,j}\ \text{(forward)} \tag{9a}$$

$$\overleftarrow{\delta}_\xi(\ )_{i,j}\equiv(\ )_{i,j}-(\ )_{i-1,j}\ \text{(backward)} \tag{9b}$$

Averaging operators, both central and one sided, are defined by

$$\mu_\xi(\ )_{i,j}\equiv\tfrac{1}{2}[(\ )_{i+1,j}+(\ )_{i-1,j}] \tag{10a}$$

$$\vec{\mu}_\xi(\ )_{i,j}\equiv\tfrac{1}{2}[(\ )_{i+1,j}+(\ )_{i,j}] \tag{10b}$$

$$\overleftarrow{\mu}_\xi(\ )_{i,j}\equiv\tfrac{1}{2}[(\ )_{i,j}+(\ )_{i-1,j}] \tag{10c}$$

**Freestream Consistency Conditions**

The conditions required to achieve zero freestream error when differencing the full-potential equation in general curvilinear coordinates ($\xi,\eta$) are now derived and discussed. Unlike the Euler equation scheme of Ref. 1, which produces zero freestream error with just a single condition, the full-potential equation, in general, requires three conditions: a condition on the metric differencing used in the density calculation and two conditions on the metric differencing used in the flux calculation. The condition on the density metric differencing is considered first.

The density is evaluated at cell centers ($i+\frac{1}{2},j+\frac{1}{2}$) in the present scheme using Eq. (3b). This relation will exactly produce (i.e., with no truncation error) the freestream value of the density $\rho_\infty$ if the quantity inside the parentheses reduces to $q_\infty^2=u_\infty^2+v_\infty^2$. The velocity potential distribution for this freestream case is given by

$$\phi=u_\infty x+v_\infty y \tag{11}$$

where $x$ and $y$ are standard Cartesian coordinates and $u_\infty$ and $v_\infty$ are the freestream velocity components along the $x$ and $y$ directions, respectively.

The quantity in the parentheses of Eq. (3b) after rearranging reduces to

$$q^2=J^2[(y_\eta\phi_\xi-y_\xi\phi_\eta)^2+(x_\xi\phi_\eta-x_\eta\phi_\xi)^2] \tag{12}$$

This expression reduces precisely to $q_\infty^2$ if the difference operators used for all $\xi$-differences involving $x$, $y$, and $\phi$ are the same, and the difference operators used for all $\eta$-differences involving $x$, $y$, and $\phi$ are the same (freestream-consistency condition number one). This can be verified easily by substituting difference operators for all derivatives into Eq. (12) and then using Eq. (11) to simplify.

One set of difference operators suitable for $x$, $y$, and $\phi$ to obtain zero freestream truncation error in the density calculations is given by

$$(\ )_\xi|_{i+\frac{1}{2},j+\frac{1}{2}}\cong\vec{\mu}_\eta\vec{\delta}_\xi(\ )_{i,j} \tag{13a}$$

$$(\ )_\eta|_{i+\frac{1}{2},j+\frac{1}{2}}\cong\vec{\mu}_\xi\vec{\delta}_\eta(\ )_{i,j} \tag{13b}$$

Even though the previous condition was derived for the case of two dimensions, the extension to three dimensions is straightforward. A similar set of difference operators for $x$, $y$, $z$, and $\phi$ used in the three-dimensional, cell-centered density calculation scheme is given by

$$(\ )_\xi|_{i+\frac{1}{2},j+\frac{1}{2},k+\frac{1}{2}}\cong\vec{\mu}_\eta\vec{\mu}_\zeta\vec{\delta}_\xi(\ )_{i,j,k} \tag{14a}$$

$$(\ )_\eta|_{i+\frac{1}{2},j+\frac{1}{2},k+\frac{1}{2}}\cong\vec{\mu}_\xi\vec{\mu}_\zeta\vec{\delta}_\eta(\ )_{i,j,k} \tag{14b}$$

$$(\ )_\zeta|_{i+\frac{1}{2},j+\frac{1}{2},k+\frac{1}{2}}\cong\vec{\mu}_\xi\vec{\mu}_\eta\vec{\delta}_\zeta(\ )_{i,j,k} \tag{14c}$$

The second and third consistency conditions for zero freestream error are associated with the flux calculation and are now discussed. Consider the full-potential equation in conservative form for general curvilinear coordinates [see Eq. (3a)]. After rearranging we have

$$\left(\frac{\xi_x\phi_x+\xi_y\phi_y}{J}\right)_\xi+\left(\frac{\eta_x\phi_x+\eta_y\phi_y}{J}\right)_\eta=0 \tag{15}$$

where the density has been dropped because of the freestream flow assumption and

$$\phi_x=\xi_x\phi_\xi+\eta_x\phi_\eta=J(y_\eta\phi_\xi-y_\xi\phi_\eta)=u \tag{16a}$$

$$\phi_y=\xi_y\phi_\xi+\eta_y\phi_\eta=J(-x_\eta\phi_\xi+x_\xi\phi_\eta)=v \tag{16b}$$

If the difference operators for the $\xi$-differences of $x$, $y$, and $\phi$ and the difference operators for the $\eta$-differences of $x$, $y$, and $\phi$ are the same, then $\phi_x = u_\infty$ and $\phi_y = v_\infty$. This is the second freestream consistency condition. Note that this condition is the same as the first condition, provided the density and flux calculations are performed at the same grid locations. However, this is not the usual case, and, therefore, these two conditions have to be satisfied independently.

With $\phi_x = u_\infty$ and $\phi_y = v_\infty$, Eq. (15) can be rewritten as

$$\left(\frac{\xi_x u_\infty + \xi_y v_\infty}{J}\right)_\xi + \left(\frac{\eta_x u_\infty + \eta_y v_\infty}{J}\right)_\eta = 0 \tag{17}$$

or by using Eq. (7) as

$$u_\infty (y_{\eta\xi} - y_{\xi\eta}) + v_\infty (x_{\eta\xi} - x_{\xi\eta}) = 0 \tag{18}$$

Thus, the finite difference operators used to obtain the metric quantities must commute. This is the third consistency condition.

One set of difference formulas used to obtain zero truncation error in the freestream flux calculation is given by

$\xi$-flux

$$(\,)_\xi\,|_{i+\frac{1}{2},j} \cong \vec{\delta}_\xi (\,)_{i,j} \tag{19a}$$

$$(\,)_\eta\,|_{i+\frac{1}{2},j} \cong \vec{\mu}_\xi \delta_\eta (\,)_{i,j} \tag{19b}$$

$\eta$-flux

$$(\,)_\xi\,|_{i,j+\frac{1}{2}} \cong \vec{\mu}_\eta \delta_\xi (\,)_{i,j} \tag{20a}$$

$$(\,)_\eta\,|_{i,j+\frac{1}{2}} \cong \vec{\delta}_\eta (\,)_{i,j} \tag{20b}$$

The second consistency condition extends to three dimensions in much the same fashion as the first does. However, extension of the third condition to three dimensions is somewhat more difficult; it requires the following three equations to be satisfied.

$$(y_\eta z_\zeta - y_\zeta z_\eta)_\xi + (y_\zeta z_\xi - y_\xi z_\zeta)_\eta + (y_\xi z_\eta - y_\eta z_\xi)_\zeta = 0 \tag{21a}$$

$$(x_\zeta z_\eta - x_\eta z_\zeta)_\xi + (x_\xi z_\zeta - x_\zeta z_\xi)_\eta + (x_\eta z_\xi - x_\xi z_\eta)_\zeta = 0 \tag{21b}$$

$$(x_\eta y_\zeta - x_\zeta y_\eta)_\xi + (x_\zeta y_\xi - x_\xi y_\zeta)_\eta + (x_\xi y_\eta - x_\eta y_\xi)_\zeta = 0 \tag{21c}$$

That is, once all the derivatives of Eq. (21) are replaced by difference operators, these relationships must cancel out just as in the analytical case.[7] Values of $A_1$, $A_2$, $A_3$, and $J$, in the two-dimensional flux calculation which satisfy both the second- and third-consistency conditions, were obtained with the same set of difference operators for all primitive metrics, $x_\xi, x_\eta$, etc. [see Eqs. (19) and (20)]. This is not the situation in three dimensions. Separate difference formulas for the primitive metrics are required to satisfy the latter two conditions. For example, the $A_1$ metric quantity can be rewritten as

$$A_1 = \xi_x \bar{\xi}_x + \xi_y \bar{\xi}_y + \xi_z \bar{\xi}_z \tag{22}$$

The quantities without bars must be computed so as to satisfy condition two, and the barred quantities must satisfy condition three.

The use of this scheme requires more storage (or a slight increase in execution time if the metrics are recomputed each step). Separate values of the metrics are required at four locations. The minimum number of arrays required for a cell-centered density algorithm (assuming all metrics are stored with no averaging) is 15 as compared to 7 for the standard three-dimensional case. If the densities are computed at the $\xi$-cell faces (i.e., at $i+\frac{1}{2},j,k$), then the storage for a perfect freestream-capture spatial difference scheme in three dimensions is reduced to 13 arrays. With the size of computer memories rapidly increasing, such a storage penalty may not be too high a price to pay for the resulting improvements in accuracy.

## Finite Difference Algorithms

Seven finite difference schemes for the conservative full-potential equation in two dimensions have been investigated in the present study. These schemes involved different variations for the calculation of flux metrics, density metrics, and density. For the sake of brevity, only three of these schemes will be presented and discussed and will involve variations in only the flux and density metric calculations. Of the three difference schemes presented, scheme 0 satisfies none of the freestream consistency conditions described in the previous section, scheme 1 satisfies only condition one, and scheme 3 satisfies all three consistency conditions. Throughout this report the designations "scheme 0, scheme 1, or scheme 3" will precisely refer to the schemes defined in the following paragraphs. The designation type 0 scheme, type 1 scheme, or type 3 scheme will refer to any scheme which satisfies none of the consistency conditions, only the first consistency condition, or all three consistency conditions, respectively.

Schemes 0 and 1 require four two-dimensional metric arrays and scheme 3 requires seven two-dimensional metric arrays. All three schemes consist of the following basic form:

$$\overleftarrow{\delta}_\xi [\rho(A_1\phi_\xi + A_2\phi_\eta)/J]_{i+\frac{1}{2},j} + \overleftarrow{\delta}_\eta [\rho(A_2\phi_\xi + A_3\phi_\eta)/J]_{i,j+\frac{1}{2}} = 0 \tag{23}$$

where the four terms in Eq. (23) represent the four mass fluxes entering or leaving the element or volume sides which surround each grid point. The density is computed at cell centers (i.e., at $i+\frac{1}{2},j+\frac{1}{2}$) and then is averaged to obtain values at $i+\frac{1}{2},j$ and $i,j+\frac{1}{2}$.

Finite difference formulas used for $\phi_\xi$ and $\phi_\eta$ in the density calculation are given by (for schemes 0, 1, or 3)

$$\phi_\xi\,|_{i+\frac{1}{2},j+\frac{1}{2}} \cong \vec{\mu}_\eta \vec{\delta}_\xi \phi_{i,j} \tag{24a}$$

$$\phi_\eta\,|_{i+\frac{1}{2},j+\frac{1}{2}} \cong \vec{\mu}_\xi \vec{\delta}_\eta \phi_{i,j} \tag{24b}$$

Finite difference formulas used in the $\xi$-flux calculations for $\phi$ are given by (for schemes 0, 1, or 3)

$$\phi_\xi\,|_{i+\frac{1}{2},j} \cong \vec{\delta}_\xi \phi_{i,j} \tag{25a}$$

$$\phi_\eta\,|_{i+\frac{1}{2},j} \cong \vec{\mu}_\xi \delta_\eta \phi_{i,j} \tag{25b}$$

For convenience, only the $\xi$-flux finite difference formulas are given. The $\eta$-flux formulas can be obtained via symmetry. The primitive metrics, $x_\xi, x_\eta$, etc., used in both the density and flux calculations for scheme 0, are computed using

$$(x \text{ or } y)_\xi\,|_{i,j} \cong \delta_\xi (x \text{ or } y)_{i,j} \tag{26a}$$

$$(x \text{ or } y)_\eta\,|_{i,j} \cong \delta_\eta (x \text{ or } y)_{i,j} \tag{26b}$$

Values of the metric quantities $A_1$, $A_2$, $A_3$, and $J$ are then formed using Eqs. (5-7) and stored at nodal points. Values of $A_1$, $A_2$, $A_3$, and $J$ required at $i+\frac{1}{2},j$, etc., and used in either the density or flux calculations, are computed using simple averages. The primitive metrics used in both the density and flux calculations for scheme 1 are computed using

$$(x \text{ or } y)_\xi\,|_{i+\frac{1}{2},j+\frac{1}{2}} \cong \vec{\mu}_\eta \vec{\delta}_\xi (x \text{ or } y)_{i,j} \tag{27a}$$

$$(x \text{ or } y)_\eta\,|_{i+\frac{1}{2},j+\frac{1}{2}} \cong \vec{\mu}_\xi \vec{\delta}_\eta (\text{x or y})_{i,j} \tag{27b}$$

Values of the metric quantities $A_1$, $A_2$, $A_3$, and $J$ are then computed using Eqs. (5−7) and stored at cell centers $(i+\frac{1}{2},j+\frac{1}{2})$. Values required at $i+\frac{1}{2},j$ or $i,j+\frac{1}{2}$ in the flux calculations are computed using simple averages.

The primitive metrics used in the density and flux calculations for scheme 3 are computed using

(for density metric calculation)

$$(x \text{ or } y)_\xi \,|_{i+\frac{1}{2},j+\frac{1}{2}} \cong \vec{\mu}_\eta \vec{\delta}_\xi (x \text{ or } y)_{i,j} \tag{28a}$$

$$(x \text{ or } y)_\eta \,|_{i+\frac{1}{2},j+\frac{1}{2}} \cong \vec{\mu}_\xi \vec{\delta}_\eta (x \text{ or } y)_{i,j} \tag{28b}$$

(for $\xi$-flux metric calculations)

$$(x \text{ or } y)_\xi \,|_{i+\frac{1}{2},j} \cong \vec{\delta}_\xi (x \text{ or } y)_{i,j} \tag{29a}$$

$$(x \text{ or } y)_\eta \,|_{i+\frac{1}{2},j} \cong \vec{\mu}_\xi \delta_\eta (x \text{ or } y)_{i,j} \tag{29b}$$

Values of $A_1$, $A_2$, $A_3$, and $J$ are computed from Eqs. (28) and (5-7) and then stored at cell centers for use in only the density calculations. Values of $(A_1/J)$ and $(A_2/J)$ are computed from Eqs. (29) and (5-7) and then stored at $\xi$-cell faces $(i+\frac{1}{2},j)$ for use in only the $\xi$-flux calculation. Values of $(A_2/J)$ and $(A_3/J)$ are required in the $\eta$-flux calculation at $i,j+\frac{1}{2}$ and are computed similarly to the $(A_1/J)$ and $(A_2/J)$ values at $i+\frac{1}{2},j$.

The next step is to compare the ability of each scheme to capture freestream on an appropriately general curvilinear grid. As a verification of the freestream consistency condition, a simple $5\times5$ grid is used to evaluate the residual (at $i=3$, $j=3$) with a freestream potential distribution imposed. The residual will indicate the amount of error due to the violation of the consistency condition.

A model grid with skewness, stretching, and a singularity at $j=3$ is examined and shown in Fig. 1a. The skewness and singularity strength are measured by the inclination $\sigma$, the amount of stretching by the stretching factor (SF), both defined in Fig. 1a. Scheme 0 suffers immediate breakdown as shown in Fig. 1b. Scheme 1 has problems for large skew angles with breakdown occurring at about $\sigma=40$ deg. Scheme 3 handles the problem with no signs of breakdown until $\sigma\cong80$ deg. Of course, at $\sigma=90$ deg the grid is completely singular with all points lying on a single straight line.

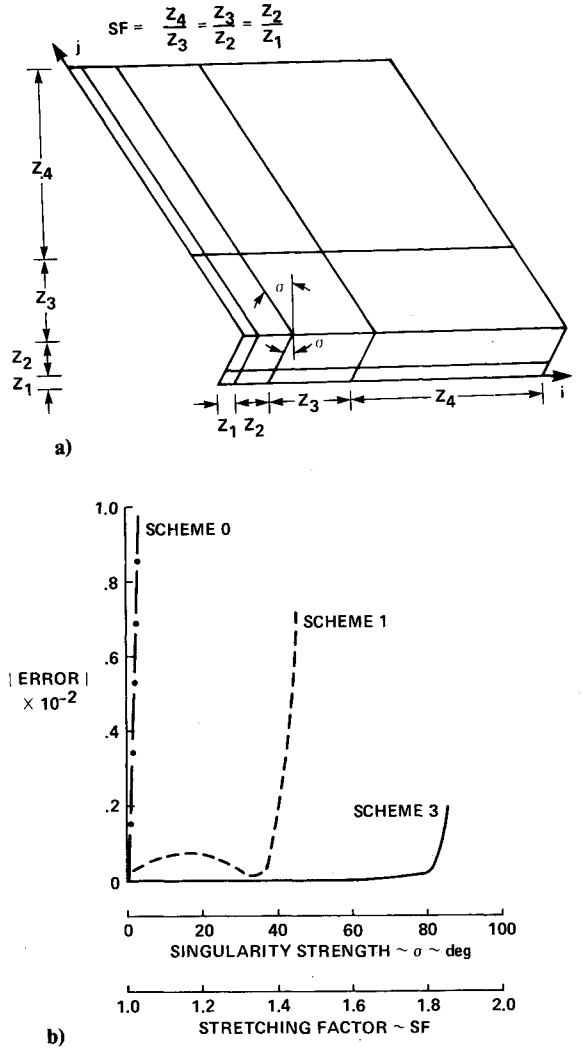


**Fig. 1 Combined singularity, skewness, and stretching test: a) sample grid; b) residual vs stretching factor (SF) and singularity strength ($\sigma$).**

## Numerical Results

Numerical results using several variations of the TAIR computer code[8] are now presented and discussed. A detailed description of the algorithm presently used in the TAIR code is given in Ref. 9. The first two variations involve basically the standard TAIR code with fourth-order accurate metrics and a slightly modified version with second-order accurate metrics. Neither of these schemes (respectively called TAIR4 and TAIR2) satisfy any consistency conditions and are, thus, of the type 0 variation. Additional results are included for schemes 1 and 3. These four versions of TAIR are used to study the effects of several different types of grid singularities on transonic flow calculations.

The model problem used is transonic flow ($M_\infty=0.45$, $\alpha=0.0$) over a circular cylinder, producing a supersonic bubble on the upper and lower surfaces which are terminated with a shock. Results on only the upper half of the plane are displayed. Results obtained on meshes with various types of irregularities are compared to a solution obtained on a regular polar mesh using the standard TAIR code.

Figure 2 illustrates the first type of irregularity studied: a single grid cell abnormality located on the vertical axis above the cylinder. Two parameters are used to characterize this singularity: 1) the ring position ($JJ$) and 2) the strength of the singularity ($S$). Both of these parameters are defined in Fig. 2.

To illustrate the local improvements in accuracy, the pressure coefficient distribution $C_p$ is plotted along the vertical axis through the top of the cylinder (Fig. 3). The abscissa is a measure of the distance from the body to the outer boundary, $Y/B=1.0$ being the outer boundary. Away from the singularity the mesh is essentially smooth and all schemes correspond accurately to the standard solution. As the singularity is approached, Fig. 3 shows that locally the accuracy of TAIR4 begins to deteriorate. This is not unexpected since the fourth-order accurate metrics will feel this singularity before the second-order metrics of TAIR2 and scheme 1. At the singularity, TAIR2, compared to the standard solution, is locally inaccurate. This is due to total neglect of the consistency conditions, as can be verified by the superior accuracy of scheme 1. Scheme 1 satisfies only the first consistency condition, yet this computationally small change has a dramatic effect on local accuracy for the present case. In other cases we shall see that all three consistency conditions are required to obtain good accuracy.

Scheme 3 results were not shown since quantitatively they were similar to scheme 1. At first glance it appeared that scheme 3 and scheme 1 should not have produced the same results for this type of singularity. However, a closer examination of the freestream residual revealed a numerical cancellation in error, associated with scheme 1, which would not occur for a general singularity.

The next type of irregularity used was a discontinuous type of stretching. Figure 4 shows the test grid, the parameters being $RM$ and $JJ$. The parameter $JJ$ has the same connotation as before. The second parameter ($RM$) defines the amount of

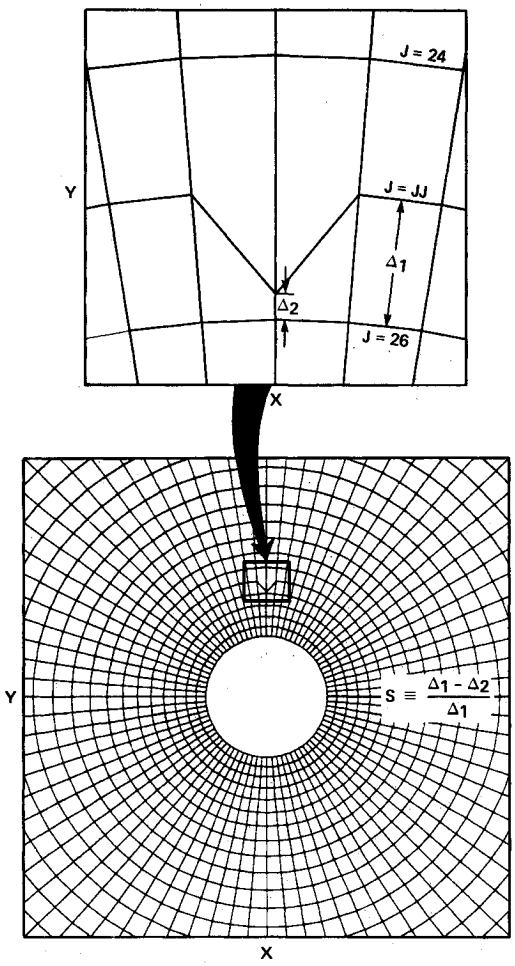


Fig. 2 Sample grid with kink for $S = 0.9$, $JJ = 25$.

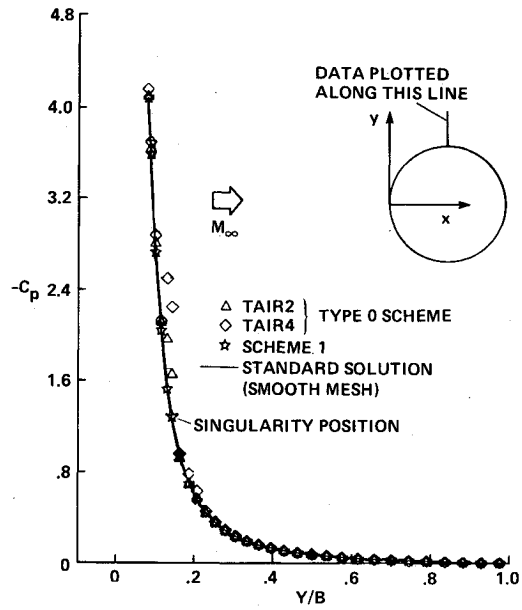


Fig. 3 $C_p$ distribution along vertical axis, $S = 0.9$, $JJ = 25$.

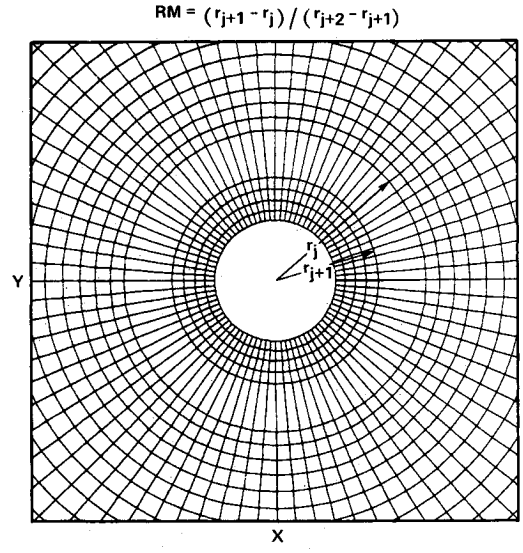


Fig. 4 Sample grid with radial spacing jump for $RM = 4.0$, $JJ = 25$.

the radial-direction spacing jump between rings $JJ$ and $JJ+1$. The rest of the mesh maintains a smooth and continuous variation.

Figure 5 shows the $C_p$ distribution for $JJ = 25$ and $RM = 4.0$ along the vertical axis. The degradation in local accuracy for TAIR2 and TAIR4 is immediately obvious. In this supersonic region the schemes are first-order accurate, due to the upwinding of the algorithm. Thus, the reduction in truncation error due to scheme 1 is reflected by its superior improvement in local accuracy.

This type of local irregularity, which encompasses the whole geometry, greatly influences the $C_p$ distribution on the cylindrical body. As Fig. 6 shows, all schemes are experiencing difficulty on the body. As expected, the TAIR2 and TAIR4 results are very inaccurate, especially in that part of the body solution where supersonic flow prevails. Scheme 1 experiences difficulties also but produces the best solution. This indicates the importance of satisfying consistency conditions as a means of controlling the truncation error near the body. That is, even though these consistency conditions were derived from freestream flow considerations, they have a significant impact in flow regions away from freestream flow. For this case, the reduction in truncation error of scheme 1 manifested itself in the superior improvement in local and global accuracy with no additional work required.

#### Airfoil Comparisons

Transonic airfoil calculations from the TAIR computer code are now presented and discussed. TAIR uses a density and metric numerical smoothing at the trailing edge of airfoils. For this study the density smoothing is disabled in order to compare it to the new schemes. Note that scheme 1 and scheme 3 have no type of density or metric smoothing. As previously mentioned, the standard TAIR code is of the scheme 0 type.

The first case tested was a Korn airfoil at design conditions ($M_\infty = 0.75$, $\alpha = 0.115$). Figure 7 shows a comparison of surface pressure coefficient distributions for three schemes: 1) the standard scheme with fourth-order accurate metrics which satisfies none of the consistency conditions, 2) a scheme which satisfies only the first-consistency condition, and 3) a scheme which satisfies all three consistency conditions. The shock is in approximately the same location for all cases. However, it is interesting to note the relative strength of each shock. We expect a shock of zero strength at these flow conditions. The strength of the shock is an estimate of the numerical error associated with each algorithm. The scheme 1 results produce the strongest shock followed in order by the TAIR4 and scheme 3 results. This order is not entirely unexpected, since in the smooth portions of the mesh the fourth-order accurate metrics should in general yield more accurate results than the second-order accurate metrics. Satisfying the first-consistency

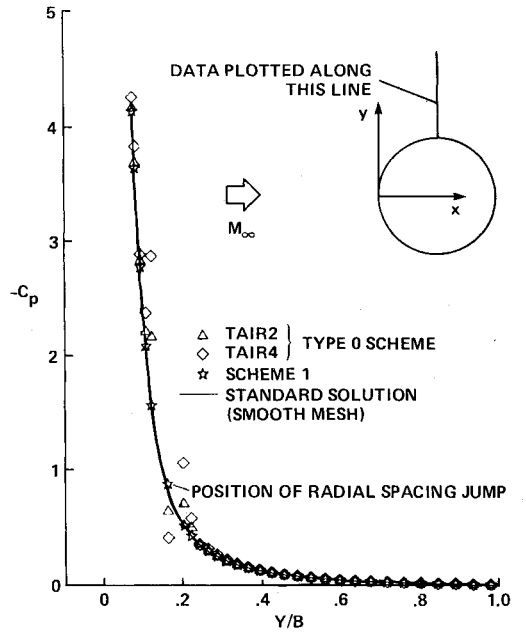


**Fig. 5 $C_p$ distribution along vertical axis, $RM = 4.0$, $JJ = 25$.**

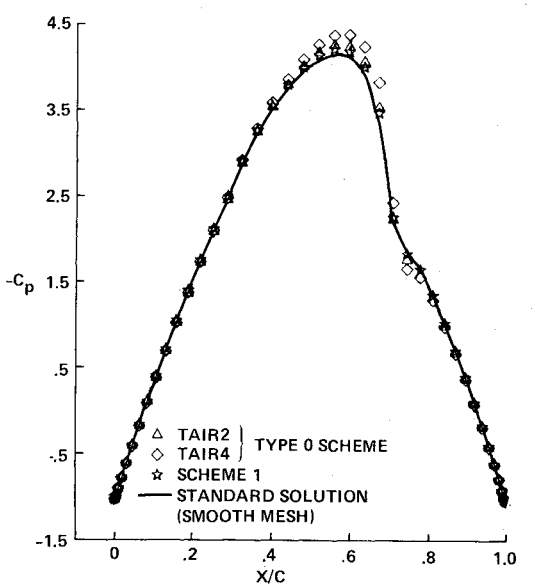


**Fig. 6 $C_p$ distribution along cylinder surface, $RM = 4.0$, $JJ = 25$.**

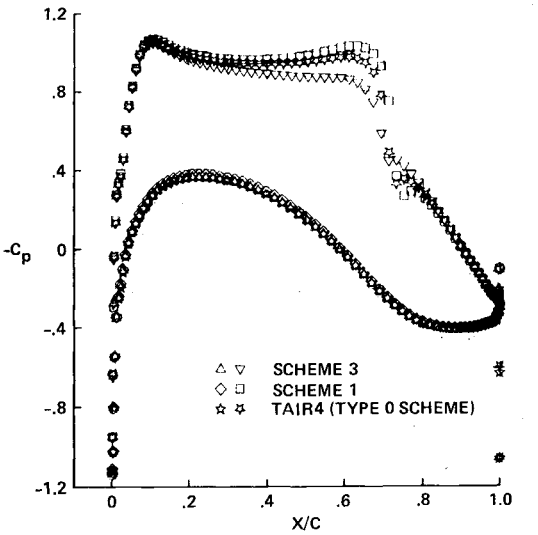


**Fig. 7 $C_p$ distribution for Korn airfoil, $M_\infty = 0.75$, $\alpha = 0.115$ deg.**

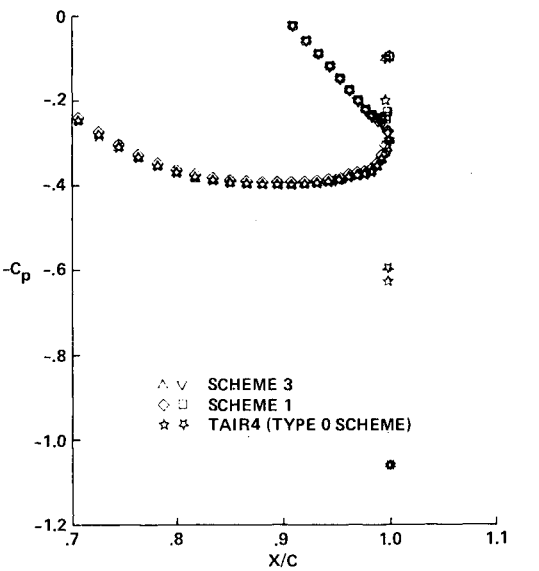


**Fig. 8 Expanded scale of trailing edge for Korn airfoil.**

condition reduces some truncation error but apparently not to the same extent as a scheme with fourth-order accurate metrics on a smooth mesh. It is interesting that scheme 3, which also has second-order accurate metrics, exhibits the most numerically accurate solution.

Figure 8 shows an expanded scale of the trailing-edge solution for the Korn airfoil just presented. The trailing-edge mapping singularity manifests itself in rapid stretching and grid skewness surrounding the trailing edge. As previously demonstrated, the local accuracy of schemes which do not satisfy the consistency conditions suffer in these areas. This trend is displayed in Fig. 8 where TAIR4 and scheme 1 both show oscillations in the solution at the trailing edge. Partial satisfaction of the consistency conditions (e.g., scheme 1) is not sufficient in this case to handle the singularity at the trailing edge. However, scheme 3 has a very smooth $C_p$ distribution around the trailing edge. This test case illustrates the superiority of scheme 3 and, in general, the advantage of satisfying all three consistency conditions.

Results from a mesh refinement study are presented next. The purpose of this study was to investigate the influence of metric differencing on the global error associated with a transonic airfoil solution. During this study, as the mesh was refined the ratio of the number of grid points along the airfoil to the number of grid points away from the airfoil was held fixed.

The lift coefficient $C_L$ is plotted vs the inverse of the number of grid points on the airfoil in Fig. 9. Three curves are displayed corresponding to the three schemes discussed in the previous section. An NACA 0012 airfoil at $M_\infty = 0.75$ and $\alpha = 2$ deg was used for all results. All three curves, representing the three different types of metric differencing, approach the same asymptotic limit as necessary to be mathematically consistent. What is interesting to note is not the final answer, but rather the rate of approach to the final answer. On coarse meshes the error associated with each of the three schemes is quite different, with scheme 3 being most accurate, TAIR4 next, and scheme 1 being least accurate. The behavior between TAIR4 and scheme 1 is unexpected, since scheme 1 satisfies consistency condition one and TAIR4 satisfies none of the consistency conditions. Apparently, the fourth-order accurate metrics associated with TAIR4 produce smaller levels of error in $C_L$ (because the mesh is reasonably

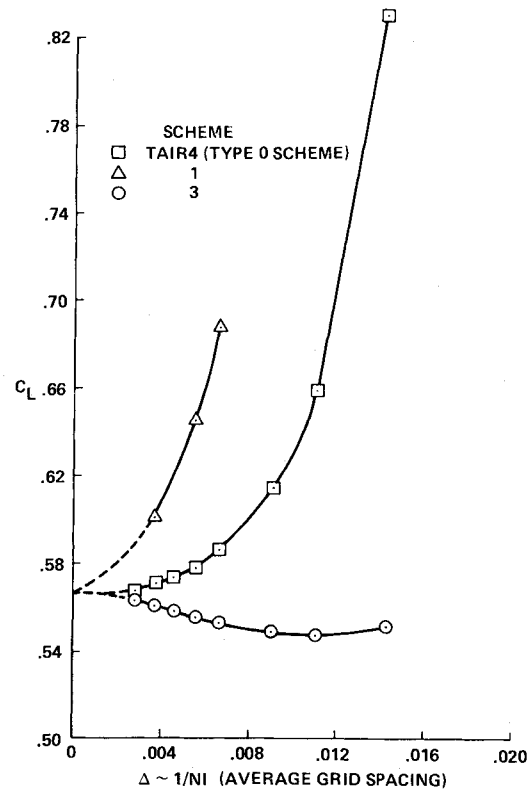


**Fig. 9** $C_L$ vs grid coarseness for NACA 0012, $M_\infty = 0.75$, $\alpha = 2$ deg.

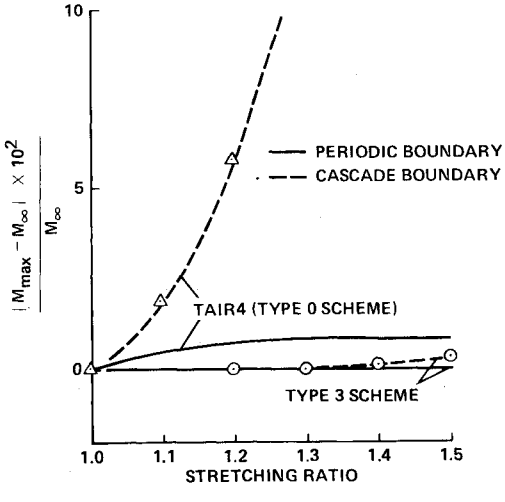


**Fig. 10 Boundary condition and freestream capturing.**

smooth) than the second-order accurate metrics of scheme 1. The scheme 3 behavior in this study indicates a vast improvement in accuracy on coarse meshes, which is a highly desirable quality in three-dimensional problems.

It should be pointed out that computer times and iteration counts were comparable for the different schemes tested in the TAIR code. Typical airfoil solution run times on the CDC 7600 computer using $149 \times 30$ meshes ranged from about 5 s for cases with small regions of supersonic flow to about 20 s for cases with large regions of supersonic flow.

#### Boundary-Condition Effect

The overall accuracy of a finite difference scheme is often lowered by the presence of computational boundaries. The freestream capturing capability can also be affected, depending on the way the boundary condition is treated. This is briefly studied by a model problem involving two different types of boundary conditions: periodic and solid wall.

A stretched Cartesian grid is generated over a flat-plate cascade. The grid is stretched so that cells with various aspect ratios are established along the boundaries. Uniform freestream is computed using this grid and two different sets of boundary conditions: 1) periodic $y$-boundary conditions for $-1 \le x \le 2$, and 2) periodic $y$-boundary conditions for $-1 < x < 0$ and $1 < x < 2$ and solid surface conditions for $0 \le x \le 1$. Condition 1 effectively simulates an infinite flowfield while condition 2 models a two-dimensional cascade geometry.

For this test, the finite volume scheme given in Ref. 5 without the so-called flux compensation terms is chosen to represent a type 3 spatial difference scheme while the TAIR4 spatial differencing scheme is used as a type 0 algorithm. The freestream capturing capability of the finite volume scheme is removed when flux compensating terms are added for the purpose of coupling odd-even points. This drawback is circumvented by utilizing a zero normal velocity condition ($V = 0$) on the solid surface instead of the flux reflection condition as commonly used in the finite volume approach. In the present study, the odd-even decoupling was not a problem because only freestream flows were computed. The coupling effect of this boundary condition is strong near the body and becomes weaker as the distance from the surface increases.

The relative error in capturing uniform freestream after convergence is shown in Fig. 10. Using condition one, the type 3 scheme reproduces uniform freestream, while TAIR4 reasonably bounds the error under various stretching ratios (Fig. 10). When condition two is imposed, the exact freestream capturing capability of the type 3 scheme is perturbed, yet the relative error is found to be very small up to a stretching ratio of 1.5. On the other hand, changing the boundary condition type contaminates the TAIR4 results substantially. In practice, the stretching ratio rarely exceeds 1.5 (using the stretching ratio of 1.5, a highly clustered boundary-layer type of grid can be generated). Therefore, the freestream capturing capability of the type 3 scheme can be regarded as satisfactory in calculating flow with boundary condition two. However, to use TAIR4, a smoothly varying grid with a very low stretching ratio is essential.

## Conclusions

Spatial difference schemes for the transonic full-potential equation involving several variations of metric differencing have been investigated. Three consistency conditions, which when satisfied produce perfect freestream capture, have been derived and presented. Comparisons of overall computing times for solutions generated by the old scheme (TAIR4) and types 1 and 3 schemes reflect no significant differences. Although the new consistency conditions have been derived for freestream flow, their implementation in non-freestream flow regions greatly improves the global accuracy. The improvement in accuracy offered by the present approach is in two forms. The local accuracy around mesh singularities is greatly improved and the global error associated with, for example, the lift is also improved. This truncation error reduction is greatest on nonsmooth, highly stretched and/or skewed meshes.

## References

[1] Pulliam, T.H. and Steger, J.L., "Implicit Finite-Difference Simulations of Three-Dimensional Compressible Flow," *AIAA Journal*, Vol. 18, Feb. 1980, pp. 159-167.

[2] Thomas, P.D. and Lombard, C.K., "The Geometric Conservation Law – A Link between Finite-Difference and Finite Volume Methods of Flow Computation on Moving Grids," AIAA Paper 78-1208, Seattle, Wash., July 1978.

[3]Hindman, R.D., "Geometrically Induced Errors and their Relationship to the Form of the Governing Equations and the Treatment of Generalized Mappings," AIAA Paper 81-1008, Palo Alto, Calif., June 1981.

[4]Chattot, J.J., Coulombeix, C., and da Silva Tome, C., "Calculs d'ecoulements Transsoniques Autour d'ailes," *La Recherche Aerospatiale,* No. 4, July-August 1978, pp. 143-159.

[5]Caughey, D.A. and Jameson, A., "Basic Advances in the Finite Volume Method for Transonic Potential Flow Calculations," presented at the Numerical and Physical Aspects of Aerodynamic Flows Symposium, California State University, Long Beach, Calif., Jan. 1981.

[6]Steger, J.L. and Baldwin, B.S., "Shock Waves and Drag in the Numerical Calculation of Isentropic Transonic Flow," NASA TN D-6997, Oct. 1972.

[7]Viviand, H., "Conservative Forms of Gas Dynamic Equations," *La Recherche Aerospatiale,* No. 1, Jan.-Feb. 1974, pp. 65-68.

[8]Dougherty, F. C., Holst, T. L., Gundy, K. L., and Thomas, S. D., "TAIR—a Transonic Airfoil Analysis Computer Code," NASA TM-81296, May 1981.

[9]Holst, T. L., "Implicit Algorithm for the Conservative Transonic Full-Potential Equation Using an Arbitrary Mesh," *AIAA Journal,* Vol. 17, Oct. 1979, pp. 1038-1045.

*From the AIAA Progress in Astronautics and Aeronautics Series...*

**SHOCK WAVES, EXPLOSIONS, AND DETONATIONS—v. 87**

**FLAMES, LASERS, AND REACTIVE SYSTEMS—v. 88**

*Edited by J. R. Bowen, University of Washington,*
*N. Manson, Université de Poitiers,*
*A. K. Oppenheim, University of California,*
*and R. I. Soloukhin, BSSR Academy of Sciences*

In recent times, many hitherto unexplored technical problems have arisen in the development of new sources of energy, in the more economical use and design of combustion energy systems, in the avoidance of hazards connected with the use of advanced fuels, in the development of more efficient modes of air transportation, in man's more extensive flights into space, and in other areas of modern life. Close examination of these problems reveals a coupled interplay between gasdynamic processes and the energetic chemical reactions that drive them. These volumes, edited by an international team of scientists working in these fields, constitute an up-to-date view of such problems and the modes of solving them, both experimental and theoretical. Especially valuable to English-speaking readers is the fact that many of the papers in these volumes emerged from the laboratories of countries around the world, from work that is seldom brought to their attention, with the result that new concepts are often found, different from the familiar mainstreams of scientific thinking in their own countries. The editors recommend these volumes to physical scientists and engineers concerned with energy systems and their applications, approached from the standpoint of gasdynamics or combustion science.

*Vol. 87—Published in 1983, 532 pp., 6×9, illus., $30.00 Mem., $45.00 List*
*Vol. 88—Published in 1983, 460 pp., 6×9, illus., $30.00 Mem., $45.00 List*
*Set—$60.00 Mem., $75.00 List*

TO ORDER WRITE: Publications Order Dept., AIAA, 1633 Broadway, New York, N.Y. 10019